iScience

CellPress

Article

Visualizing Ligand Binding to a GPCR *In Vivo* Using NanoBRET

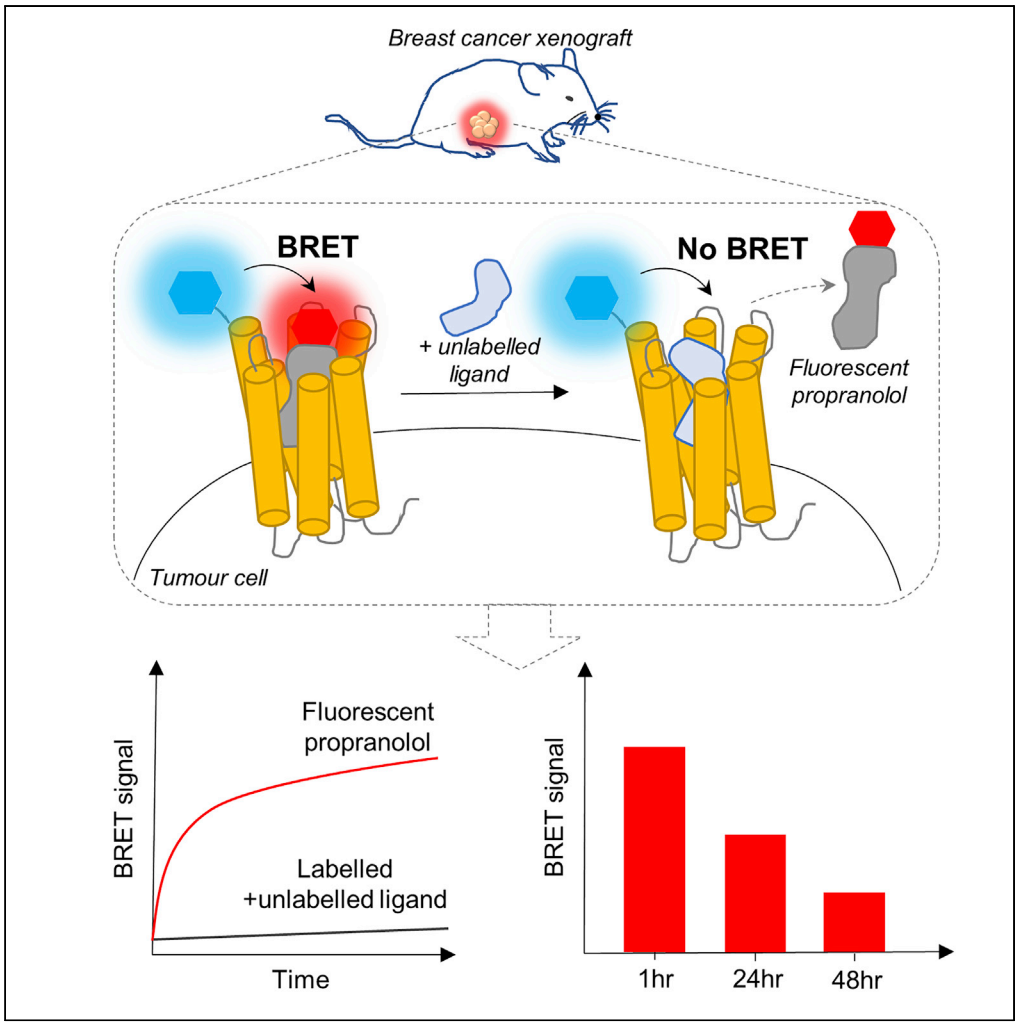

Diana C. Alcobia, Alexandra I. Ziegler, Alexander Kondrashov, ..., Jeanette Woolard, Stephen J. Hill, Erica K. Sloan

jeanette.woolard@nottingham.ac.uk (J.W.)
steve.hill@nottingham.ac.uk (S.J.H.)
erica.sloan@monash.edu (E.K.S.)

HIGHLIGHTS

NanoLuc luciferase was used to localize β_2-adrenoceptors *in vivo*

Metastatic breast cancer cells retain expression of β_2-adrenoceptors

The binding of fluorescent propranolol to β_2-adrenoceptors was quantified *in vivo*

NanoBRET was used to monitor target engagement in a mouse model of breast cancer

Alcobia et al., iScience 6, 280–288
August 31, 2018
https://doi.org/10.1016/j.isci.2018.08.006

iScience

CellPress

Article

Visualizing Ligand Binding to a GPCR *In Vivo* Using NanoBRET

Diana C. Alcobia,[1,2,5] Alexandra I. Ziegler,[5] Alexander Kondrashov,[3] Eleonora Comeo,[2,4] Sarah Mistry,[2,4] Barrie Kellam,[2,4] Aeson Chang,[5] Jeanette Woolard,[1,2,*] Stephen J. Hill,[1,2,8,*] and Erica K. Sloan[5,6,7,*]

SUMMARY

The therapeutic action of a drug depends on its ability to engage with its molecular target *in vivo*. However, current drug discovery strategies quantify drug levels within organs rather than determining the binding of drugs directly to their specific molecular targets *in vivo*. This is a particular problem for assessing the therapeutic potential of drugs that target malignant tumors where access and binding may be impaired by disrupted vasculature and local hypoxia. Here we have used triple-negative human breast cancer cells expressing β_2-adrenoceptors tagged with the bioluminescence protein NanoLuc to provide a bioluminescence resonance energy transfer approach to directly quantify ligand binding to a G protein-coupled receptor *in vivo* using a mouse model of breast cancer.

INTRODUCTION

G protein-coupled receptors (GPCRs) comprise the largest family of cell surface receptors involved in signal transduction (Santos et al., 2017; Wacker et al., 2017). In recent years, there has been a realization that a number of GPCRs may play important roles in cancer (Nieto Gutierrez and McDonald, 2018; De Francesco et al., 2017; Bar-Shavit et al., 2016; Liu et al., 2016; O'Hayre et al., 2013). For example, β-adrenoceptors are intimately involved in the pathogenesis of infantile hemangioma (Leaute-Labreze et al., 2008; Stiles et al., 2012) and have been implicated in the progression of several malignant tumor types including angiosarcoma, breast cancer, and ovarian cancer (Rains et al., 2017; Watkins et al., 2015; Armaiz-Pena et al., 2013; Choy et al., 2016; Le et al., 2016; Sloan et al., 2010). In particular, activation of β_2-adrenoceptors by physiological stress can switch cancer cells to an invasive metastatic phenotype (Sloan et al., 2010; Chang et al., 2016; Creed et al., 2015). The classical β-adrenoceptor antagonist, propranolol, has clinical efficacy for the treatment of infantile hemangiomas and angiosarcomas (Leaute-Labreze et al., 2008, 2015; Chow et al., 2015; Stiles et al., 2013) and prevents the progression of cancer in mouse models (Sloan et al., 2010) and in patients (Shaashua et al., 2017; De Giorgi et al., 2018).

Most cells in the body are close to vasculature allowing easy access of drugs from circulation. However, in tumors, hypoxic regions and tortured non-functional vasculature (Folkman, 1971; Ferrara, 2001; Carmeliet and Jain, 2011; Wong et al., 2015) result in a population of cells that are distant from blood vessels (Carmeliet and Jain, 2011; Minchinton and Tannock, 2006). This distance may hinder the extent to which drugs reach these cells and interact with their molecular target (Minchinton and Tannock, 2006). However, up until now there has been no simple way to visualize directly the extent to which target engagement has been achieved *in vivo*.

One approach to monitor ligand binding to GPCRs in living cells is through the use of fluorescent ligands (Baker et al., 2011; Vernall et al., 2014; Stoddart et al., 2016). However, uptake into cells can often lead to high levels of non-specific binding. We have recently dramatically improved the study of fluorescent ligand binding by developing a bioluminescence resonance energy transfer (BRET) assay that requires close proximity (*circa* 10 nm) between the fluorescent ligand and the target receptor to generate a measurable signal (Stoddart et al., 2015, 2018). This has been achieved using GPCRs tagged with a very bright luciferase (NanoLuc; Stoddart et al., 2015, 2018). This technological advance allowed us to monitor binding to the human β_2-adrenoceptor in real time using a red fluorescent analog of the antagonist propranolol, propranolol-(β-Ala-β-Ala)-X-BODIPY 630/650 (Prop-BY630; Stoddart et al., 2015; Figure S1). Here we have used this fluorescent ligand in conjunction with a triple-negative human breast cell line (MDA-MB-231^{HM}) expressing an N-terminal NanoLuc-tagged human β_2-adrenoceptor to quantify ligand binding (using NanoBRET) to a GPCR *in vivo* using a mouse model of breast cancer.

[1]Division of Physiology, Pharmacology and Neuroscience, School of Life Sciences, University of Nottingham, Nottingham NG7 2UH, UK

[2]Centre of Membrane Proteins and Receptors, University of Birmingham and University of Nottingham, The Midlands, UK

[3]Wolfson Centre for Stem Cells, Tissue Engineering & Modelling (STEM), Centre for Biomolecular Sciences, University of Nottingham, Nottingham NG7 2RD, UK

[4]School of Pharmacy, Division of Biomolecular Science and Medicinal Chemistry, Centre for Biomolecular Sciences, University of Nottingham, Nottingham NG7 2RD, UK

[5]Drug Discovery Biology, Monash Institute of Pharmaceutical Sciences, Monash University, Parkville, VIC 3052, Australia

[6]Cousins Center for Neuroimmunology, Semel Institute for Neuroscience and Human Behavior, Jonsson Comprehensive Cancer Center, and UCLA AIDS Institute, University of California Los Angeles, Los Angeles, CA 90095, USA

[7]Division of Surgical Oncology, Peter MacCallum Cancer Centre, Victorian Comprehensive Cancer Centre, 305 Grattan Street, Melbourne, VIC 3000, Australia

[8]Lead Contact

*Correspondence: jeanette.woolard@nottingham.ac.uk (J.W.), steve.hill@nottingham.ac.uk (S.J.H.), erica.sloan@monash.edu (E.K.S.)

https://doi.org/10.1016/j.isci.2018.08.006

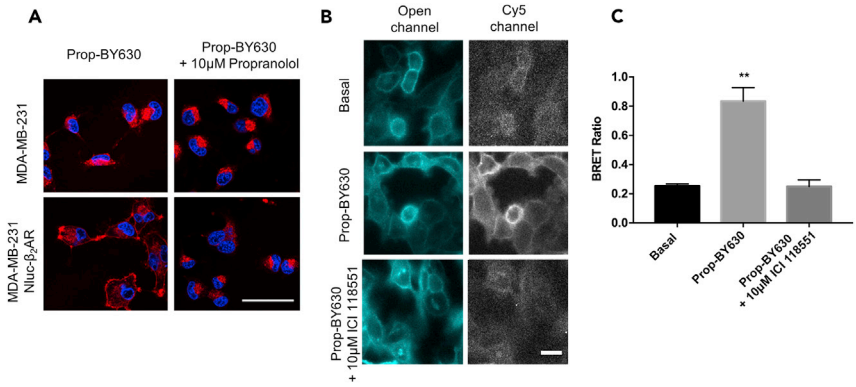

Figure 1. Binding of Fluorescent Propranolol (Propranolol-(β-Ala-β-Ala)-X-BODIPY630/650; Prop-BY630) to Triple-Negative Human Breast Cancer Cells (MDA-MB-231^{HM} cells)

(A) Fluorescence imaging of the binding of 50 nM Prop-BY630 to non-transfected MDA-MB-231^{HM} cells (upper panels) or MDA-MB-231^{HM} cells expressing NanoLuc-tagged human β_2-adrenoceptors (lower panels). Cells were pre-treated with Hoechst 33342 nuclear stain (2 μg/mL; blue labeling) and then labeled for 30 min with Prop-BY630 (red labeling). Upper right and bottom right panels show cells pre-incubated with 10 μM unlabelled propranolol before labeling with fluorescent propranolol (50 nM Prop-BY630). Cells were washed just before imaging to remove unbound fluorescent ligand. Data are representative images from 3 independent experiments. Scale bar represents 50μm.

(B) Bioluminescence imaging (Olympus LV200) of NanoLuc-tagged β_2-adrenoceptors. MDA-MB-231^{HM} Nluc-β_2AR cells treated with 400 nM furimazine substrate alone (upper panels) to detect luminescence in the absence of added fluorescent ligand using an open channel (20 s exposure time; 420 nm longpass filter; upper left panel) or a Cy5 channel (4 min exposure time; 600/50 nm bandpass filter; upper right panel) to detect BRET generated by binding of fluorescent ligand, when present. Middle and lower panels show images from cells treated with 50 nM Prop-BY630, in the presence (lower panels) or absence (middle panels) of unlabelled ICI 118551 (10 μM). Images shown were acquired with an open channel (middle and lower left panels) and the Cy5 channel (middle and lower right panels). Scale bar represents 50 μm.

(C) BRET ratios obtained using bioluminescence imaging using ImageJ time series analyzer. Data show the mean and SE obtained in 3 independent experiments. **$p < 0.01$ compared with basal or in the presence of 10 μM ICI 118551 (one-way ANOVA with Tukey's multiple comparisons).

RESULTS AND DISCUSSION

We began by generating an MDA-MB-231^{HM} cell line stably expressing the human β_2-adrenoceptor with an N-terminal NanoLuc tag. Standard fluorescence confocal microscopy revealed some of the limitations of using a fluorescent probe without BRET (Figure 1A). Thus, following incubation with a fluorescent analog of the β-blocker propranolol (50 nM; Prop-BY630; Figure S1), fluorescence was detected by confocal imaging at both the cell membrane and in a discrete perinuclear region (Figure 1A; lower left panel). Cell membrane fluorescence was completely prevented by co-incubation with 10 μM unlabelled propranolol (Figure 1A; lower right panel), demonstrating specific binding of the ligand to the β_2-adrenoceptors on the cell surface. Perinuclear labeling, however, was not displaced by co-incubation with 10 μM unlabelled propranolol indicating non-specific binding. Furthermore, only non-specific binding was detected in non-transfected MDA-MB-231^{HM} cells (Figure 1A; upper left panel). This demonstrates that although confocal microscopy can detect cell surface receptors using fluorescent ligands, interpretation of the fluorescence readout may be confounded in an *in vivo* setting by the extent of non-specific binding to non-receptor sites.

To determine if BRET with NanoLuc-tagged receptors in combination with fluorescent ligands had the specificity required to detect ligand-binding to GPCRs on the surface of cancer cells, we first used wide-field bioluminescence imaging to demonstrate the cell membrane location of the NanoLuc-tagged β_2-adrenoceptor in MDA-MB-231^{HM} cells (Figure 1B; left panels). Addition of 50 nM Prop-BY630 allowed us to visualize the energy transfer from the N-terminal NanoLuc of the β_2-adrenoceptor to the fluorescent ligand bound to the receptor via NanoBRET (detected in the Cy5 channel). This clearly revealed specific binding to cell surface β_2-adrenoceptors that could be inhibited by a selective β_2-antagonist ICI 118551 (10 μM; $p < 0.001$; Figures 1B and 1C). The BRET signal from this ligand-receptor interaction was also measured in a 96-well plate format using a CLARIOstar plate reader, and demonstrated that the specific binding detected by BRET increased with the concentration of the probe until all of the receptors on the cell surface had been occupied. This specific binding (the difference between total binding and

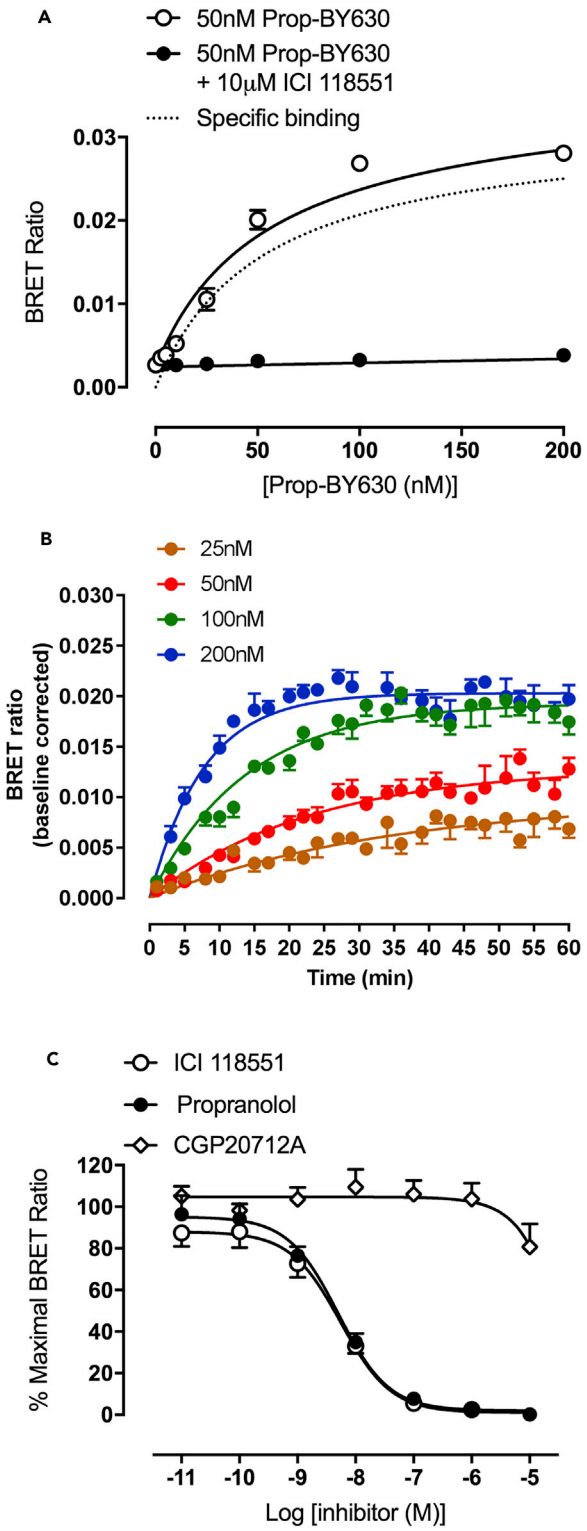

Figure 2. Quantitative Analysis of Ligand Binding to NanoLuc-Tagged Human β_2-Adrenoceptors Expressed in MDA-MB-231^{HM} Cells Using NanoBRET

(A) Binding of increasing concentrations of Propranolol-(β-Ala-β-Ala)-X-BODIPY630/650 (Prop-BY630) to NanoLuc-tagged human β_2-adrenoceptors in MDA-MB-231^{HM} cells measured using a CLARIOstar plate reader. Non-specific binding was defined with 10 μM unlabelled ICI 118551. Data are mean ± SE from 6 separate experiments. Total

Figure 2. *Continued*
(open circles) and non-specific binding (closed circles) curves were fitted simultaneously as described in the Transparent Methods. The dotted line shows the specific binding component derived from this analysis.
(B) Real-time kinetic analyses of Prop-BY630 binding to NanoLuc-tagged human β_2-adrenoceptors expressed in MDA-MB-231^{HM} cells using 25, 50, 100, and 200 nM fluorescent ligand. BRET ratios for kinetic studies have been baseline-corrected to specific binding (after subtraction of non-specific binding) at time 0. Data are mean ± SE of triplicate determinations in a representative experiment. Similar data were obtained in 4 additional experiments.
(C) Inhibition of the specific binding of 50 nM Prop-BY630 to NanoLuc-tagged human β_2-adrenoceptors in MDA-MB-231^{HM} cells by increasing the concentrations of ICI 118551, un-labelled propranolol, and CGP20712A. Data are mean ± SE from 5 separate experiments.

non-specific binding) was clearly saturable (pK_D = 7.28 ± 0.07; n = 5; Figure 2A) and equally important for the future *in vivo* experiments; non-specific binding to non-receptor sites (obtained in the presence of 10 μM ICI 118551) was very low (Figure 2A; closed circles).

To determine the compatibility for *in vivo* studies, we also imaged the BRET signal using a whole-animal bioluminescence and fluorescence imaging system, IVIS Lumina II (Figure S2A), and obtained a comparable pK_D for fluorescent propranolol (7.26 ± 0.06, n = 5). This was consistent with the value obtained previously for this ligand in HEK293 cells (Stoddart et al., 2015). The BRET methodology also allowed us to determine the binding kinetics of fluorescent propranolol (k_{on} 5.4 ± 2.2 × 10^5 M^{-1} min^{-1}; k_{off} 0.025 ± 0.004 min^{-1}; n = 5; Figure 2B). This confirmed that Prop-BY630 could bind rapidly to the β_2-adrenoceptor, but once bound dissociated slowly (the reciprocal of k_{off} gives a residence time of 40 min), making it an ideal probe for *in vivo* use. Similar data for ligand binding kinetics/residence time were obtained in separate experiments using the IVIS system (Figure S2B).

To ensure that the BRET signal detected was confined to the β_2-adrenoceptor, competition-binding experiments were undertaken with the β_2-adrenoceptor-selective antagonist ICI 118 551, the β_1-selective antagonist CGP 20712A (Gherbi et al., 2015), and the non-selective β-blocker propranolol (Figure 2C). These experiments yielded pK_i values that were consistent with literature values obtained previously for binding to β_2-adrenoceptors (Stoddart et al., 2015; Figures 2C, S2C, and S2D; Table S1). Thus, the β_1-selective antagonist CGP 20712A produced very little inhibition of fluorescent ligand binding at concentrations up to 10 μM (Figure 2C). These data confirm that this BRET proximity assay is exquisitely selective and only detects binding to NanoLuc-tagged β_2-adrenoceptors expressed on the tumor cells. Furthermore, our data also confirmed that the optical properties of the IVIS system had the sensitivity to detect ligand binding to β_2-adrenoceptors on cancer cells by BRET (Figure S2).

Previous work from our laboratory has shown that β_2-adrenoceptors on MDA-MB-231^{HM} cells may play a significant role in the effect of stress on metastasis (Le et al., 2016; Sloan et al., 2010; Chang et al., 2016). Those studies used tumor cells that had been transfected with a cytosolic firefly luciferase marker to monitor primary tumor growth and metastasis in a mouse model of breast cancer (Le et al., 2016; Sloan et al., 2010; Chang et al., 2016). Cytosolic NanoLuc luciferase has also been used to monitor cancer progression in living animals (Stacer et al., 2013). In contrast, here we used receptor-specific NanoLuc bioluminescence to localize *in vivo* tumor cells that specifically express β_2-adrenoceptors. In mice injected with tumor cells into the mammary fat pad, luminescence intensity from NanoLuc-β_2-adrenoceptors (photons/sec) increased from 8 days after tumor cell injection (Figures 3A and 3B) and correlated with primary tumor size determined by caliper (mm^3; Pearson correlation: $p < 0.0001$, $R^2 = 0.560$; Figure 3A). Metastatic tumors containing cells expressing β_2-adrenoceptors appeared in the lung and axillary lymph nodes later in tumor development (Figure 3C).

To detect ligand binding *in vivo* by BRET we injected Prop-BY630 (0.1 mg/kg) directly into the tumor (intratumoral [IT]) and used the IVIS Lumina II imaging system to monitor the red fluorescence emission from the fluorescent ligand relative to the blue luminescence donor emission from the NanoLuc-labeled β2-adrenoceptors. This ratiometric approach determines the level of specific ligand binding independently of the number of cells expressing NanoLuc-β_2-adrenoceptors present in the tumor. Thus, regardless of the slight variation in tumor burden between mice, we were able to compare how well Prop-BY630 interacted with the target β_2-adrenoceptor on tumor cells. Preliminary experiments established that addition of 0.1 mg/kg Prop-BY630 delivered directly into the tumor reached a steady plateau BRET ratio, significantly above baseline values (n = 7; $p < 0.001$; two-way ANOVA), within *circa* 15 min of administration of the fluorescent ligand (Figure S3).

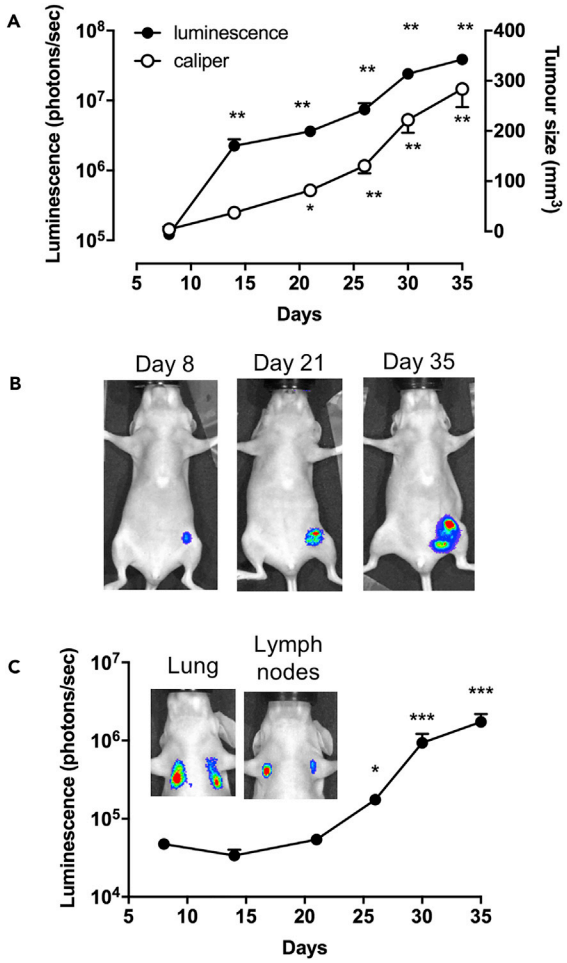

Figure 3. Whole-Animal Bioluminescence Imaging of NanoLuc-β_2AR MDA-MB-231^{HM} Tumor Growth and Metastasis Development

(A) Female BALB/c nu/nu mice (7-week-old) were injected in the fourth left mammary fat pad with 5 × 10^5 MDA-MB-231^{HM} triple-negative human breast cancer cells that stably express the NanoLuc-tagged human β_2-adrenoceptor. Tumor development was monitored by bioluminescence imaging (left y axis) 5 min after IV injection of the NanoLuc substrate furimazine (100 μL in PBS, *circa* 0.37 mg/kg) or by caliper measurements (right y axis) over 35 days.

(B) Representative bioluminescence images of primary tumors.

(C) Bioluminescence monitoring of the development of metastasis in lungs and axillary lymph nodes. Inset: representative images of lung and lymph node metastasis. Data were obtained from 11 mice and are expressed as mean ± SE. *$p < 0.05$, **$p < 0.005$, ***$p < 0.0001$ (two-way ANOVA with Tukey's multiple comparisons with respect to day 8 baseline). For luminescence measurements, the statistical analysis was applied to the log transformed values.

In a separate experiment with a crossover design, administration of the fluorescent ligand significantly increased the BRET ratios for each mouse (measured after 1 hr), demonstrating detection of specific ligand binding to β_2-adrenoceptors (Figures 4A and 4C; $p < 0.0001$). Receptor engagement by the fluorescent ligand was prevented by pre-treating mice with the β_2-selective antagonist ICI 118551, delivered either directly into the tumor (0.3 mg/kg IT $p < 0.0001$; Figures 4A and 4B) or through the tail vein (10 mg/kg intravenously [IV] $p < 0.001$; Figures 4C and 4D), demonstrating that the assay can be used to quantify the extent to which unlabeled drugs (e.g., ICI 118551) can engage with their molecular target when delivered directly into the tumor or through the circulation.

Drug-receptor engagement in the primary tumor region was also investigated for a lower dose of ICI 118551 administered IV (1 mg/kg), as well as for the β_1-selective antagonist CGP20712A (10 mg/kg IV; 100 μL in PBS) (Figure 5). These experiments demonstrated that pre-treatment with CGP20712A produced no significant attenuation of the specific binding of Prop-BY630 to β_2-adrenoceptors on MDA-MB-231^{HM}

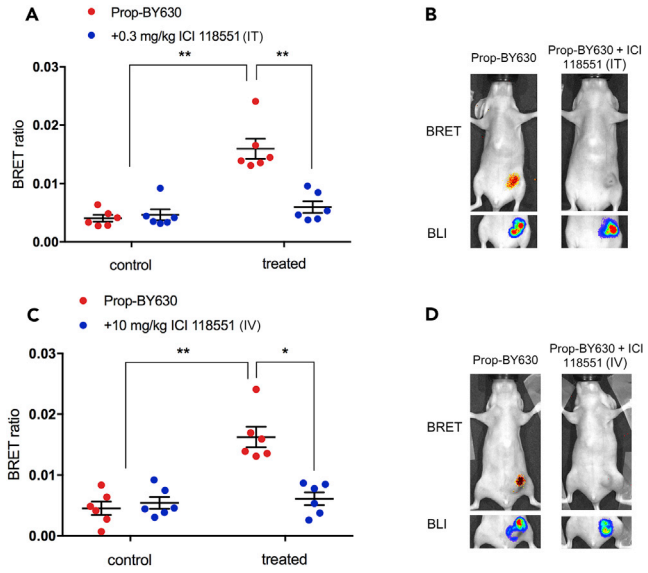

Figure 4. NanoBRET to Monitor Specific Ligand-Receptor Binding *In Vivo* in Primary MDA-MB-231^{HM} Tumors

(A) Female BALB/c nu/nu mice (7-week-old) were injected in the fourth left mammary fat pad with 5 × 10^5 MDA-MB-231 triple-negative human breast cancer cells stably expressing Nluc-β_2AR. Once tumor size reached >200 mm^3; BRET ratios were determined from mice administered fluorescent propranolol-(β-Ala-β-Ala)-X-BODIPY630/650 alone (Prop-BY630 at 0.1 mg/kg intra-tumor, IT; red circles) or from mice receiving both Prop-BY630 (0.1 mg/kg IT) and 0.3 mg/kg ICI 118551 (IT; blue circles). ICI 118551 was administered 45 min before the fluorescent propranolol. Control represents measurements taken 5 min after IV injection (in 100 μL; *circa* 0.37 mg/kg) of the furimazine substrate 24 hr before administration of any β_2-adrenoceptor-directed ligands. BRET measurements of ligand binding were made 1 hr after injection of Prop-BY630 (treated condition). Furimazine substrate was injected IV 5 min before mice were imaged. Data represent mean ± SE of 6 mice in each group. **$p < 0.0001$ (two-way ANOVA with Tukey's multiple comparison test) compared with both control datasets and the 1 hr treatment with Prop-BY630.

(B) Representative images showing single mice exposed to Prop-BY630 only (left panel) or to 0.3 mg/kg (IT) ICI 118551 and 0.1 mg/kg (IT) Prop-BY630 (right panel). Upper panels shown in (B) show BRET images and lower panels show the total bioluminescence (BLI) from the NanoLuc.

(C) BRET ratios determined from mice administered with fluorescent ligand alone (Prop-BY630 0.1 mg/kg IT; red circles) or from mice receiving both Prop-BY630 (0.1 mg/kg IT) and 10 mg/kg ICI 118551 (IV; blue circles). **$p<0.0001$ (two-way ANOVA with Tukey's multiple comparison test) compared with both control datasets. *$p<0.001$ compared to 1h treatment with Prop-BY630.

(D) Representative images showing mice exposed to 0.1 mg/kg Prop-BY630 (IT) alone or to 10 mg/kg ICI 118551 (IV) and 0.1 mg/kg Prop-BY630. Data represent mean ± SE of 6 mice in each group.

tumors *in vivo*, whereas a 10-fold lower dose of the β_2-selective antagonist ICI 118551 produced a significant inhibition ($p < 0.05$; Figures 5; compare Figure 4B). These data demonstrate the ability of this assay to accurately report target engagement *in vivo*. The data obtained with ICI 188551 indicate that 1 mg/kg (IV) is a dose that achieves roughly 50% target engagement of tumor cell β_2-adrenoceptors within this solid breast cancer tumor model (Figure 5).

Finally, to establish the sensitivity of the assay to different doses of the fluorescent ligand, we monitored *in vivo* ligand-binding BRET responses following addition of 0.01, 0.03, or 0.1 mg/kg of Prop-BY630 and quantified the *in vivo* receptor residence times over 72 hr (Figure 6). These experiments demonstrated significant ligand binding that could be detected by BRET with all 3 doses of the fluorescent ligand in a dose-dependent manner (Figure 6). Furthermore, binding of each of the 3 doses of Prop-BY630 to tumor β_2-adrenoceptors was maintained for at least 48 hr after initial drug application (Figure 6). These data are consistent with the slow off-rate kinetics of Prop-BY630 from the β2-adrenoceptor observed *in vitro* (Figure 2) and also suggest that the drug is not rapidly cleared from the tumor environment.

The close proximity requirements (10 nm) for BRET to occur between the donor NanoLuc on the N-terminus of human β_2-adrenoceptors on tumor cells and the receptor-bound Prop-BY630 therefore provides a very sensitive and selective ligand binding assay to monitor receptor target engagement in tumors *in vivo*. As a

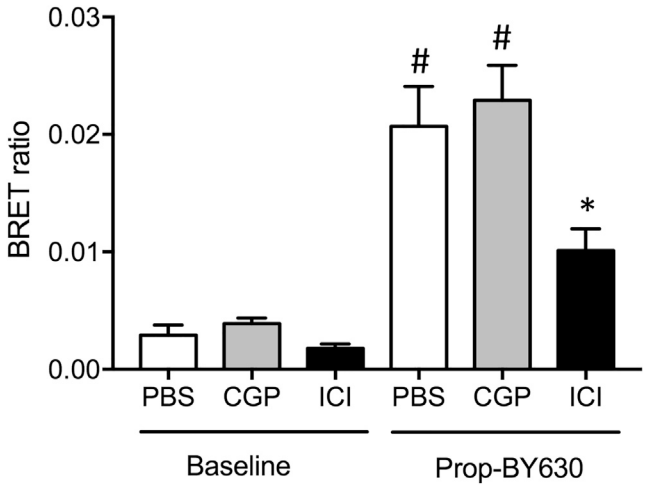

Figure 5. Effect of Selective β_1- and β_2-Adrenoceptor Antagonists on Prop-BY630 Binding to MDA-MB-231^{HM} Cells *In Vivo*

Drug-receptor engagement in the primary tumor region was investigated using 0.1 mg/kg (IT) Prop-BY630 in mice treated with the β_2-selective antagonist ICI 118551 or the β_1-selective antagonist CGP20712A. At 45 min before fluorescent ligand injection, mice were administered (IV) with either PBS (100 μL), CGP201712A (100 μL; 10 mg/kg in PBS), or ICI 118551 (100 μL; 1 mg/kg in PBS). Data represent mean ± SE of 6 mice in each group. Measurements were made 1 hr after administration of Prop-BY630. Baseline measurements were obtained on the previous day in each mouse when furimazine was administered via the tail vein, but Prop-BY630 was not injected into the tumor. *$p < 0.05$ or $^{\#}p < 0.001$ with respect to the baseline (t = 0) signal in each group. *$p < 0.05$ versus control Prop-BY630 binding (1 hr PBS). One-way ANOVA with Tukey's posthoc tests.

consequence, the BRET readout should not be influenced by fluorescent ligand binding to neighboring endogenous receptors on other cell types (e.g., vascular and immune cells) within the tumor microenvironment. We therefore believe that this approach has significant advantages in specificity over other *in vivo* imaging modalities such as positron emission tomography (Hazan et al., 2017) for the study of specific receptor target engagement in tumors.

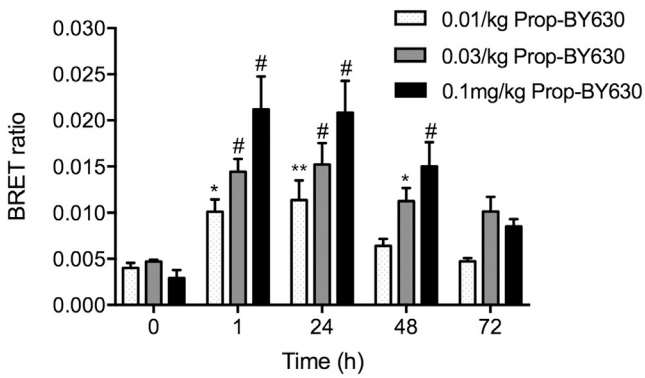

Figure 6. Dose-Dependent Binding of Prop-BY630 to β_2-Adrenoceptors and Subsequent Ligand Dissociation *In Vivo*

To monitor fluorescent ligand dissociation over time in the primary tumors, mice were administered with 3 different doses of propranolol-(β-Ala-β-Ala)-X-BY630/650 (0.01, 0.03, or 0.1 mg/kg; IT). At 1, 24, 48, and 72 hr after fluorescent ligand injection, mice were injected with furimazine substrate (IV, 100 μL in PBS, *circa* 0.37 mg/kg) and imaged 5 min later using the IVIS Lumina II camera system. Imaging was performed by capturing sequential luminescence (open channel, 30 s exposure time) and fluorescence (Cy5.5 channel, 5 min exposure times) images. All mice were also imaged on the day before fluorescent ligand injection following an IV injection of furimazine to determine luminescence (and BRET) baseline (t = 0). Data represent mean ± SE of 6 mice in each group. *$p < 0.05$. **$p < 0.01$ or $^{\#}p < 0.001$ compared with corresponding time 0 controls. Two-way ANOVA with repeated measures and Dunnett multiple comparisons.

In summary, the present study has shown that ligand binding to a GPCR can be monitored *in vivo* using BRET. Here we have used triple-negative human breast cancer cells expressing human β_2-adrenoceptors tagged with the bioluminescence protein NanoLuc to demonstrate that parenterally applied drugs can access receptors on tumor cells in a mouse model of breast cancer. This *in vivo* NanoBRET method will be widely applicable to monitor target engagement in animal models for other cell surface receptors such as receptor tyrosine kinases (Kilpatrick et al., 2017) and for intracellular kinases (Robers et al., 2015).

Limitations of Study

The resolution of *in vivo* nanoBRET was limited in the present study to the detection of established tumors including macro-metastases. Future development of fluorescent ligands with increased water solubility should increase the stability in plasma and improve the detection of IV-administered probes. The development of new nanoluciferase substrates should also improve the *in vivo* detection of resonance energy transfer.

METHODS

All methods can be found in the accompanying Transparent Methods supplemental file.

SUPPLEMENTAL INFORMATION

Supplemental Information includes Transparent Methods, three figures, and one table and can be found with this article online at https://doi.org/10.1016/j.isci.2018.08.006.

ACKNOWLEDGMENTS

We acknowledge the assistance of Mr. Cameron Nowell of the Monash Institute of Pharmaceutical Sciences Biomedical Imaging Facility. We thank Drs. Leigh Stoddart, Karolina Gherbi, and David James (University of Nottingham) for providing the sig-SNAP-ADRB2-pcDNA3.1(+), sig-NLuc-ADRB2-pcDNA3.1(+), and pSIN-eGFP-BSD plasmids, respectively. This work was supported by the Medical Research Council (grant number MR/N020081/1), the National Cancer Institute (CA160890), the National Health and Medical Research Council (APP1147498), the University of Birmingham and University of Nottingham Center of Membrane Proteins and Receptors, and the David and Lorelle Skewes Foundation. E.C. was an Erasmus + Visiting Researcher from the School of Pharmacy, Biotechnology & Sport Science, University of Bologna, Italy, between February and May 2017.

AUTHOR CONTRIBUTIONS

Research design: J.W., S.J.H., E.K.S.; Supervised the overall project: E.K.S., S.J.H.; Synthesized propranolol-(β-Ala-β-Ala)-X-BODIPY630/650: E.C., S.M., B.K.; Produced the pSIN-NLuc-ADRB2 expression plasmid: A.K.; Conducted experiments: D.C.A., A.C., A.I.Z., E.K.S.; Performed data analysis: D.C.A., A.C., A.I.Z., S.J.H., E.K.S.; Wrote the manuscript: D.C.A., J.W., S.J.H., E.K.S.

DECLARATIONS OF INTEREST

E.K.S. is a member of the scientific advisory board of Cyngal Therapeutics, The authors declare no other conflicts of interest.

Received: March 8, 2018
Revised: July 5, 2018
Accepted: August 7, 2018
Published: August 31, 2018

REFERENCES

Armaiz-Pena, G.N., Allen, J.K., Cruz, A., Stone, R.L., Nick, A.M., Lin, Y.G., Han, L.Y., Mangala, L.S., Villares, G.J., Vivas-Mejia, P., et al. (2013). Src activation by beta-adrenoreceptors is a key switch for tumour metastasis. Nat. Commun. *4*, 1403.

Baker, J.G., Adams, L., Salchow, K., Mistry, S., Middleton, R., Hill, S.J., and Kellam, B. (2011). Synthesis and characterization of high-affinity 4,4-difluoro-4-bora-3a,4a-diaza-s-indacene (BODIPY)-labelled fluorescent ligands for human beta-adrenoceptors. J. Med. Chem. *54*, 6874–6887.

Bar-Shavit, R., Maoz, M., Kancharla, A., Nag, J.K., Agranovich, D., Grisaru-Granovsky, S., and Uziely, B. (2016). G protein-coupled receptors in cancer. Int. J. Mol. Sci. *17*, 1320.

Carmeliet, P., and Jain, R.K. (2011). Molecular mechanisms and clinical applications of angiogenesis. Nature *7347*, 298–307.

Chang, A., Le, C.P., Walker, A.K., Creed, S.J., Pon, C.K., Albold, S., Carroll, D., Halls, M.L., Lane, J.R., Riedel, B., et al. (2016). β2-adrenoceptors on tumor cells play a critical role in stress-enhanced metastasis in a mouse model of breast cancer. Brain Behav. Immun. *57*, 106–115.

Chow, W., Amaya, C.N., Rains, S., Chow, M., Dickenson, E.B., and Bryan, B.A. (2015). Growth attenuation of cutaneous angiosarcoma with propranolol mediated beta-blockade. JAMA Dermatol. *151*, 1226–1229.

Choy, C., Raytis, J.L., Smith, D.D., Duenas, M., Neman, J., Jandial, R., and Lew, M.W. (2016). Inhibition of beta2-adrenergic receptor reduces triple-negative breast cancer brain metastases: the potential benefit of perioperative beta-blockade. Oncol. Rep. *35*, 3135–3142.

Creed, S.J., Le, C.P., Hassan, M., Pon, C.K., Albold, S., Chan, K.T., Berginski, M.E., Huang, Z., Bear, J.E., Lane, J.R., et al. (2015). β2-adrenoceptor signaling regulates invadopodia formation to enhance tumor cell invasion. Breast Cancer Res. *17*, 145.

De Francesco, E.M., Sotgia, F., Clarke, R.B., Lidanti, M.P., and Maggiolini, M. (2017). G protein-coupled receptors at the crossroad between physiologic and pathologic angiogenesis: old paradigms and emerging concepts. Int. J. Mol. Sci. *18*, 2713.

De Giorgi, V., Grazzini, M., Benemei, S., Marchionni, N., Botteri, E., Pennacchioli, E., Geppetti, P., and Gandini, S. (2018). Propranolol for off-label treatment of patients with melanoma. Results from a cohort study. JAMA Oncol. *4*, e172908.

Ferrara, N. (2001). Role of vascular endothelial growth factor in regulation of physiological angiogenesis. Am. J. Physiol. Cell Physiol. *280*, C1358–C1366.

Folkman, J. (1971). Tumor angiogenesis: therapeutic implications. N. Engl. J. Med. *285*, 1182–1186.

Gherbi, K., May, L.T., Baker, J.G., Briddon, S.J., and Hill, S.J. (2015). Negative cooperativity across β_1-adrenoceptor homodimers provides insights into the nature of the secondary low affinity "CGP 12177" β_1-adrenoceptor binding conformation. FASEB J. *29*, 2859–2871.

Hazan, P.P., Pandey, A., Chaturvedi, S., and Mishra, A.K. (2017). New trends and current status of positron-emission tomography and single-photon-emission computerized tomography radioligands for neuronal serotonin receptors and serotonin transporter. Bioconjug. Chem. *28*, 2647–2672.

Kilpatrick, L.E., Friedman-Ohana, R., Alcobia, D.C., Riching, K., Peach, C.J., Wheal, A.J., Briddon, S.J., Robers, M.B., Zimmerman, K., Machleidt, T., et al. (2017). Real-time analysis of the binding of fluorescent $VEGF_{165}$a to VEGFR2 in living cells: effect of receptor tyrosine kinase inhibitors and fate of internalized agonist-receptor complexes. Biochem. Pharmacol. *136*, 62–75.

Le, C.P., Nowell, C.J., Kim-Fuchs, C., Botteri, E., Hiller, J.G., Ismail, H., Pimentel, M.A., Chai, M.G., Karnezis, T., Rotmensz, N., et al. (2016). Chronic stress in mice remodels lymph vasculature to promote tumour cell dissemination. Nat. Commun. *7*, 10634.

Leaute-Labreze, C., Hoeger, P., Mazereeuw-Hautier, J., Guibaud, L., Baselga, E., Posiunas, G., Phillips, R.J., Caceres, H., Lopez Gutierrez, J.C., Ballona, R., et al. (2015). A randomized, controlled trial of oral propranolol in infantile hemangioma. N. Engl. J. Med. *372*, 735–746.

Leaute-Labreze, C., Dumas de la Roche, E., Hubiche, T., Boralevi, F., Thambo, J.B., and Taieb, A. (2008). Propranolol for severe hemangiomas of infancy. N. Engl. J. Med. *358*, 2649–2651.

Liu, Y., An, S., Ward, R., Yang, Y., Guo, X.X., Li, W., and Xu, T.R. (2016). G protein-coupled receptors as promising cancer targets. Cancer Lett. *376*, 226–239.

Minchinton, A.I., and Tannock, I.F. (2006). Drug penetration in solid tumours. Nat. Rev. Cancer *6*, 583–592.

Nieto Gutierrez, A., and McDonald, P.H. (2018). GPCRs: emerging anti-cancer drug targets. Cell. Signal. *41*, 65–74.

O'Hayre, M., Vázquez-Prado, J., Kufareva, I., Stawiski, E.W., Handel, T.M., Seshagiri, S., and Gutkind, J.S. (2013). The emerging mutational landscape of G proteins and G-protein coupled receptors in cancer. Nat. Rev. Cancer *13*, 412–424.

Rains, S.L., Amaya, C.N., and Bryan, B.A. (2017). Beta-adrenergic receptors are expressed across diverse cancers. Oncoscience *4*, 95–105.

Robers, M.B., Dart, M.L., Woodroofe, C.C., Zimprich, C.A., Kirkland, T.A., Machleidt, T., Kupcho, C.R., Levin, S., Hartnett, J.R., Zimmerman, K., et al. (2015). Target engagement and drug residence time can be observed in living cells with BRET. Nat. Commun. *6*, 10091.

Santos, R., Ursu, O., Gaulton, A., Bento, A.P., Donadi, R.S., Bologa, C.G., Karlsson, A., Al-Lazikani, B., Hersey, A., Oprea, T.I., et al. (2017). A comprehensive map of molecular drug targets. Nat. Rev. Drug Discov. *16*, 19–34.

Shaashua, L., Shabat-Simon, M., Haldar, R., Matzner, P., Zmora, O., Shabtai, M., Sharon, E., Allweis, T., Barshack, I., Hayman, C., et al. (2017). Perioperative COX-2 and β-adrenergic blockade improves metastatic biomarkers in breast cancer patients in a phase-II randomized trial. Clin. Cancer Res. *23*, 4651–4661.

Sloan, E.K., Priceman, S.J., Cox, B.F., Yu, S., Pimentel, M.A., Tangkanangnukul, V., Arevalo, J.M., Morizono, M., Karanikolas, B.D.W., Yu, L., et al. (2010). The sympathetic nervous system induces a metastatic switch in primary breast cancer. Cancer Res. *70*, 7042–7052.

Stacer, A.C., Nyati, S., Moudgil, P., Iyengar, R., Luker, K.E., Rehemtulla, A., and Luker, G.D. (2013). NanoLuc reporter for dual luciferase imaging in living animals. Mol. Imaging *12*, 1–13.

Stiles, J., Amaya, C., Pham, R., Rowntree, R.K., Lacaze, M., Mulne, A., Bischoff, J., Kokta, V., Boucheron, L., et al. (2012). Propranolol treatment of infantile hemangioma endothelial cells: a molecular analysis. Exp. Ther. Med. *4*, 594–604.

Stiles, J.M., Amaya, C., Rains, S., Diaz, D., Pham, R., Battiste, J., Modiano, J.F., Kokta, V., Boucheron, L., et al. (2013). Targeting of beta adrenergic receptors results in therapeutic efficacy against models of hemangioendothelioma and angiosarcoma. PLoS One *8*, e60021.

Stoddart, L.A., Johnstone, E.K.M., Wheal, A.J., Goulding, J., Robers, M.B., Machleidt, T., Wood, K.V., Hill, S.J., and Pfleger, K.D.G. (2015). Application of BRET to monitor ligand binding to GPCRs. Nat. Methods *12*, 661–663.

Stoddart, L.A., Kilpatrick, L.E., and Hill, S.J. (2018). NanoBRET approaches to study ligand binding to GPCRs and RTKs. Trends Pharmacol. Sci. *39*, 136–147.

Stoddart, L.A., White, C.W., Niguyen, Y., Hill, S.J., and Pfleger, K.D. (2016). Fluorescence and bioluminescence based approaches to study GPCR ligand binding. Br. J. Pharmacol. *173*, 3028–3037.

Vernall, A.J., Hill, S.J., and Kellam, B. (2014). The evolving small-molecule fluorescent conjugate toolbox for class A GPCRs. Br. J. Pharmacol. *171*, 1073–1084.

Wacker, D., Stevens, R.C., and Roth, B.L. (2017). How ligands illuminate GPCR molecular pharmacology. Cell *170*, 414–427.

Watkins, J.L., Thaker, P.H., Nick, A.M., Ramondetta, L.M., Kumar, S., Urbauer, D.L., Matsuo, K., Squires, K.C., Coleman, R.L., Lutgendorf, S.K., et al. (2015). Clinical impact of selective and nonselective beta-blockers on survival in patients with ovarian cancer. Cancer *121*, 3444–3451.

Wong, P.P., Demircioglu, F., Ghazaly, E., Alrawashdeh, W., Stratford, M.R., Scudamore, C.L., Cereser, B., Crnogorac-Jurcevic, T., McDonald, S., Elia, G., et al. (2015). Dual-action combination therapy enhances angiogenesis while reducing tumor growth and spread. Cancer Cell *27*, 123–137.

ISCI, Volume *6*

Supplemental Information

Visualizing Ligand Binding to a GPCR *In Vivo* Using NanoBRET

Diana C. Alcobia, Alexandra I. Ziegler, Alexander Kondrashov, Eleonora Comeo, Sarah Mistry, Barrie Kellam, Aeson Chang, Jeanette Woolard, Stephen J. Hill, and Erica K. Sloan

Supplemental Information

Visualising ligand-binding to a GPCR *in vivo* using nanoBRET.

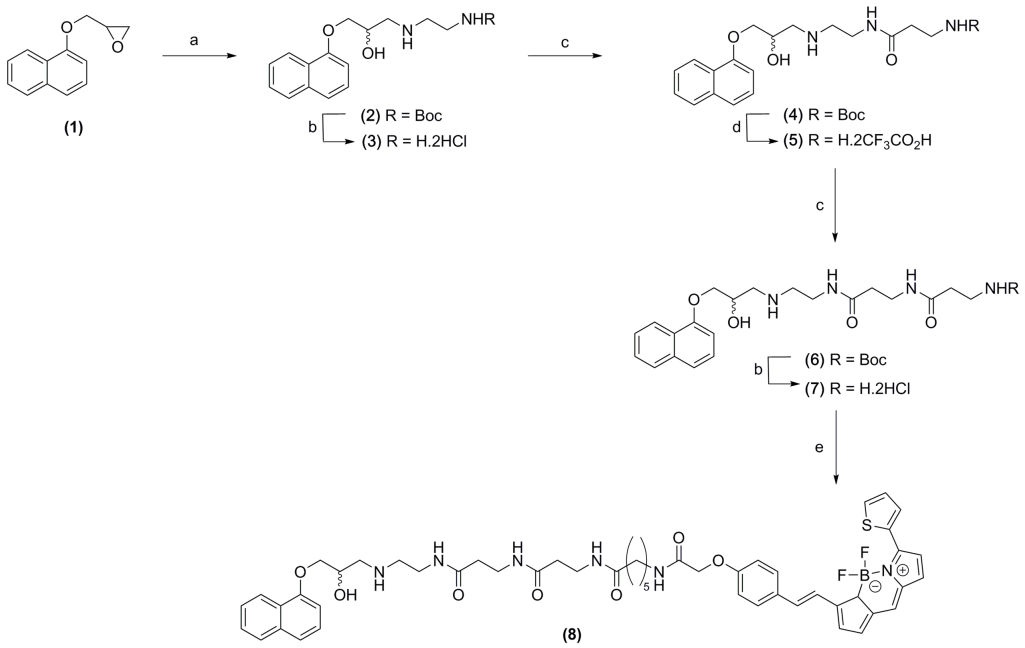

Figure S1. Reaction scheme for the synthesis of Propranolol-(β-Ala-β-Ala)-X-BODIPY630/650 (Compound 8 in the figure; Prop-BY630). Related to Figure 1.
Reagents and conditions: (a) tert-Butyl-2-aminoethyl carbamate (Boc), DMF/water (9:1), 85°C, 16h, 39%; (b) 4M HCl in dioxane, 5h, 29-100%; (c) Boc-β-Ala-OH, HBTU, DIPEA, DMF, room temperature, 35-41%; (d) TFA, DCM, room temperature, 2h, 100%; (e) BODIPY630/650-X-SE, DIPEA, DMF, room termperature, 3h, 91%. Abbreviations: BODIPY 630/650-X-SE, 6-(((4,4-difluoro-5-(2-thienyl)-4-bora-3a,4a-diaza-s-indacene-3-yl)-styryloxy)acetyl)aminohexanoic acid succinimidyl ester; DCM, dichloromethane; DIPEA, diisopropylethylamine; DMF, *N,N*-dimethylformamide; HBTU, *N,N,N′,N′*-Tetramethyl-*O*-(1*H*-benzotriazol-1-yl)uronium hexafluorophosphate; TFA, trifluoroacetic acid.

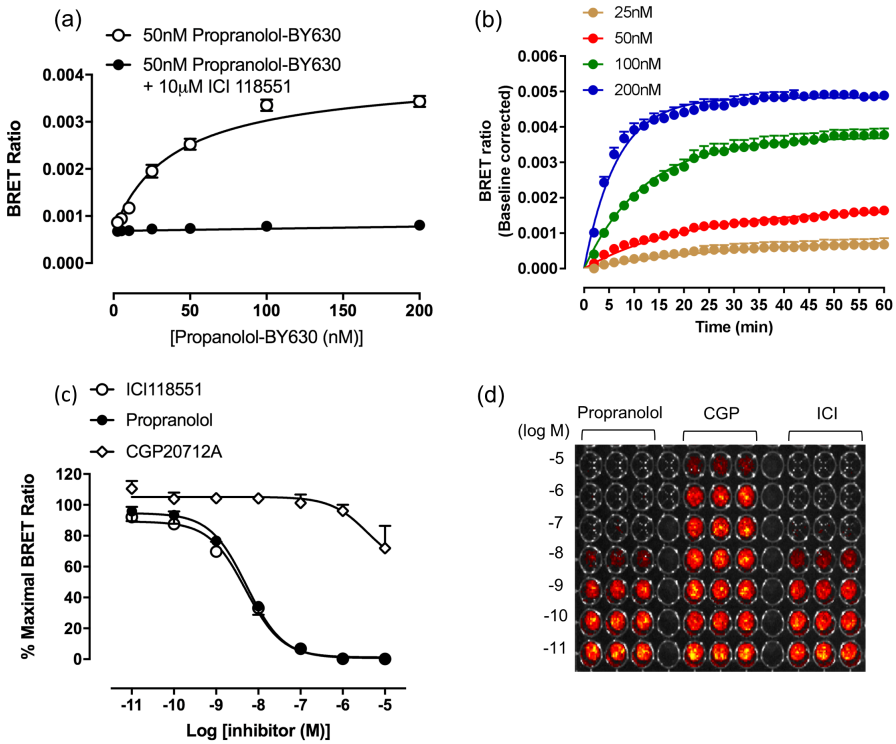

Figure S2. Quantitative analysis of ligand-binding to NanoLuc-tagged human β_2-adrenoceptors expressed in MDA-MB-231^{HM} cells using BRET imaging with the IVIS lumina II system. Related to Figure 2. (a) Binding of increasing concentrations of Propranolol-(β-Ala-β-Ala)-X-BODIPY630/650 (Prop-BY630) to NanoLuc-tagged human β_2-adrenoceptors in MDA-MB-231^{HM} cells measured using the IVIS lumina II camera system. Non-specific binding was defined with 10μM unlabelled ICI 118551. Data are mean ± S.E. of triplicate determinations in a representative experiment. Similar data were obtained in four further experiments. (b) Real time kinetic studies of Prop-BY630 binding to NanoLuc-tagged human β_2-adrenoceptors expressed in MDA-MB-231^{HM} cells using 25, 50, 100 and 200nM fluorescent ligand. Data are mean ± S.E. of triplicate determinations in a representative experiment. BRET ratios for kinetic studies have been baseline-corrected to the specific binding (after subtraction of non-specific binding) BRET ratio obtained at time zero. Similar data were obtained in two further experiments. (c) Inhibition of the specific binding of 50nM Prop-BY630 to NanoLuc-tagged human β_2-adrenoceptors in MDA-MB-231^{HM} cells by increasing concentrations of ICI 118551, propranolol and CGP20712A. Data are mean ± S.E. from four separate experiments. (d) Representative plate image obtained using the IVIS system (using the Cy5.5 emission channel) for the competition binding assay shown in (c) with ICI 118551 (ICI), propranolol and CGP 20712A (CGP).

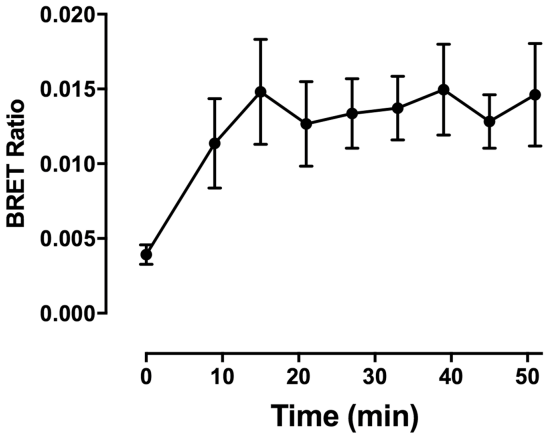

Figure S3. Time course of the binding of Prop-BY630 to β_2-adrenoceptors in vivo. Related to Figure 4. Mice were injected with 0.1 mg/kg Propranolol-(β-Ala-β-Ala)-X-630/650 (in 50μl of PBS) directly into the primary tumour (intratumoral; i.t). Immediately following this, mice were injected with 100μL 1:20 dilution furimazine substrate via the tail vein (i.v., 100μL diluted in PBS; *circa* 0.37 mg/kg) and imaged using the IVIS lumina II camera system. Mice were kept under 2-3% isoflurane anaesthesia during injections and imaging. Sequential luminescence (open channel, 30 sec exposure time) and fluorescence (Cy5.5. channel using 660/20nm bandpass filter; 5 min exposure time) images were taken every 6 min for a total time of 49 min. Images were acquired from 1 min after fluorescent ligand injection. Values show mean ± S.E from seven mice. 2-Way ANOVA confirmed that there was a significant time-dependent effect ($p<0.001$).

Table S1. Table of pK_i values obtained from competition experiments using the CLARIOstar plate reader or the IVIS imaging camera system. Related to Figure 2.

Unlabelled Ligands	CLARIOStar pK_i (mean ± S.E)	n	IVIS pK_i (mean ± S.E)	n
ICI 118551	8.55 ± 0.05	5	8.55 ± 0.02	4
Propranolol	8.68 ± 0.17	5	8.69 ± 0.18	4

Equilibrium binding parameters obtained from inhibition of the specific binding of 50nM Prop-BY630 to NanoLuc-tagged human β_2-adrenoceptors in MDA-MB-231^{HM} cells by increasing concentrations of ICI 118551 and un-labelled propranolol. Data are mean $\pm$ S.E. from n separate experiments.

TRANSPARENT METHODS

Experimental Procedures.

Synthesis of Propranolol-β-ala-β-ala-BODIPY 630/650.

Propranolol-(β-alanine,β-alanine)-X-BODIPY630/650 (Stoddart et al., 2015; Soave et al., 2016) was synthesised as described in the reaction scheme in Supplementary Figure S1.

Chemicals and solvents of analytical and HPLC grade were purchased from commercial suppliers and used without further purification. BODIPY-630/650-X-SE was purchased from Molecular Probes (Thermo Fisher Scientific). All reactions were carried out at ambient temperature unless otherwise stated. Reactions were monitored by thin-layer chromatography on commercially available silica pre-coated aluminium-backed plates (Merck Kieselgel 60 F254). Visualisation was under UV light (254 nm and 366 nm), followed by staining with ninhydrin or $KMnO_4$ dips. Flash column chromatography was performed using silica gel 60, 230-400 mesh particle size (Sigma Aldrich). NMR spectra were recorded on a Bruker-AV 400. ^{1}H spectra were recorded at 400.13 Hz and ^{13}C NMR spectra at 101.62 Hz. All ^{13}C NMR are ^{1}H broadband decoupled. Solvents used for NMR analysis (reference peaks listed) were $CDCl_3$ supplied by Cambridge Isotope Laboratories Inc., (δ_H = 7.26 ppm, δ_C = 77.16) and CD_3OD supplied by VWR (δ_H = 3.31 ppm and δ_C = 49.00). Chemical shifts (δ) are recorded in parts per million (ppm) and coupling constants are recorded in Hz. The following abbreviations are used to described signal shapes and multiplicities; singlet (s), doublet (d), triplet (t), quadruplet (q), broad (br), dd (doublet of doublets), ddd (double doublet of doublets), dtd (double triplet of doublets) and multiplet (m). Spectra were assigned using appropriate COSY and HSQC experiments. Processing of the NMR data was carried out using the NMR software Topspin 3.0. LC-MS spectra were recorded on a Shimadzu UFLCXR system coupled to an Applied Biosystems API2000 and visualised at 254 nm (channel 1) and 220 nm (channel 2). LC-MS was carried out using a Phenomenex Gemini-NX C18 110A, column (50 mm × 2 mm x 3 µm) at a flow rate 0.5 mL/min over a 5 min period (Method A). All high resolution mass spectra (HRMS) were recorded on a Bruker microTOF mass spectrometer using MS electrospray ionization operating in positive ion mode. RP-HPLC was performed on a Waters 515 LC system and monitored using a Waters 996 photodiode array detector at wavelengths between 190 and 800 nm. Spectra were analysed using Millenium 32 software. Semi-preparative HPLC was performed using YMC-Pack C8 column (150 mm × 10 mm × 5 µm) at a flow rate of 5.0 mL/min using a gradient method of 40-95% B over 15 minutes (Solvent A = 0.01% formic acid in H_2O, solvent B = 0.01% formic acid in CH_3CN (Method B)). Analytical RP-HPLC was performed using a YMC-Pack C8 column (150 mm × 4.6 mm × 5 µm) and a Phenomenex Gemini NX-C18 column

(250 mm × 4.6 mm × 5 µm) at a flow rate of 1.0 mL/min. Final products were one single peak and >95% pure. The retention time of the final product is reported using a gradient method of 5-95% solvent B in solvent A over 25 minutes. (Solvent A = 0.01% formic acid in H_2O, solvent B = 0.01% formic acid in CH_3CN (Method C)).

Abbreviations; BODIPY 630/650-X-SE, 6-(((4,4-difluoro-5-(2-thienyl)-4-bora-3a,4a-diaza-s-indacene-3-yl)-styryloxy)acetyl)aminohexanoic acid succinimidyl ester; DCM, dichloromethane; DIPEA, diisopropylethylamine; DMF, *N,N*-dimethylformamide; HBTU, *N,N,N′,N′*-Tetramethyl-*O*-(1*H*-benzotriazol-1-yl)uronium hexafluorophosphate; TFA, trifluoroacetic acid.

(±)-2-((Naphthalen-1-yloxy)methyl)oxirane (1)

The title compound was synthesised as previously described in the literature (Baker et al., 2011).

(±)-*tert*-Butyl 2-(2-hydroxy-3-(naphthalen-1-yloxy)propylamino)ethylcarbamate (2)

A solution of (±)-2-((naphthalen-1-yloxy)methyl)oxirane **(1)** (0.241 g, 1.20 mmol) and *tert*-butyl-2-aminoethylcarbamate (0.482 g, 3.01 mmol) in a mixture of DMF/water 9:1 (6 mL), was heated at 85°C for 16 hours. The solvent was removed under reduced pressure and the crude product was purified by column chromatography on silica (3% 1M NH_3 in MeOH/DCM). The title compound was afforded as an off-white solid (0.168g, 39%). ^{1}H NMR (400 MHz, $CDCl_3$) δ 8.30 – 8.18 (m, 1H), 7.84 – 7.76 (m, 1H), 7.54 – 7.41 (m, 3H), 7.36 (dd, *J* = 8.3, 7.5 Hz, 1H), 6.82 (dd, *J* = 7.6 Hz, *J* = 1.0 Hz, 1H), 4.95 (t, *J* = 5.3 Hz, 1H), 4.28 – 4.22 (m, 1H), 4.22-4.11 (m, 2H) 3.34 – 3.22(m, 2H) 3.00 (dd, *J* = 12.3, 3.7 Hz, 1H), 2.92 (dd, *J* = 12.2, 7.5 Hz, 1H), 2.83 (ddd, *J* = 6.2, 1.5 Hz, 2H), 1.44 (s, 9H). ^{13}C NMR (101 MHz, $CDCl_3$) δ 156.41, 154.36, 134.63, 127.68, 126.60, 125.94, 125.65, 125.45, 121.91, 120.85, 105.08, 70.62, 68.59, 53.57, 51.90, 49.52, 28.55. LC-MS *m/z* calc. for $C_{20}H_{29}N_2O_4$ $[MH]^+$; 361.2, found; 361.2, t_R = 2.29 min.

(±)-2-(2-Hydroxy-3-(naphthalen-1-yloxy)propyl-amino)ethylamine dihydrochloride (3)

To a solution of (±)-*tert*-butyl 2-(2-hydroxy-3-(naphthalen-1-yloxy)propyl-amino)ethylcarbamate (**2)** (0.063 g, 0.18 mmol) in Et_2O (0.5 mL) 4M HCl in dioxane (0.5 mL) was added and the mixture was stirred for 5 hours. The solvent was removed under reduced pressure to afford the title compound as a pale pink solid (0.060 g, 100%). ^{1}H NMR (400 MHz, CD_3OD) δ 8.36 – 8.26 (m, 1H), 7.86 – 7.78 (m, 1H), 7.58 – 7.43 (m, 3H), 7.39 (dd, *J* = 8.3, 7.6 Hz, 1H), 6.95 (dd, *J* = 7.6 Hz, 1H), 4.64-4.41 (m, *J* = 9.8 Hz, 1H), 4.27 (dd, *J* = 10.0, 5.0 Hz, 1H), 4.21 (dd, *J* = 10.0, 5.5 Hz, 1H), 3.57 – 3.45 (m, 3H), 3.43 – 3.35 (m, 3H). ^{13}C NMR (101 MHz, CD_3OD) δ 155.35, 136.08, 128.59, 127.51, 126.92, 126.79, 126.28, 122.80,

121.98, 106.16, 71.05, 66.84, 51.97, 45.82, 36.69. LC-MS *m/z* calc. for $C_{15}H_{21}N_2O_2$ $[MH]^+$; 261.2, found; 261.2, t_R = 0.62 min.

(±)-*tert*-Butyl(3-((2-((2-hydroxy-3-(naphthalen-1-yloxy)propyl)amino)ethyl)amino)-3-oxopropyl)carbamate (4)

To Boc-β-Ala-OH (0.090 g, 0.47 mmol) in DMF (2 mL) HBTU (0.213 g, 0.56 mmol) and DIPEA (0.302 g, 2.34 mmol) were added. The mixture was stirred for 10 minutes and (±)-2-(2-Hydroxy-3-(naphthalen-1-yloxy)propyl-amino)ethylamine dihydrochloride (**3)** (0.060 g, 0.18 mmol) in DMF (1.5 mL) was added. After stirring for 2 hours the reaction mixture was partitioned between EtOAc and a 1:1 mixture of sat. $NaHCO_{3\,(aq)}$/water. The aqueous layer was washed with EtOAc x2 and the combined organic phases were dried over $MgSO_4$, filtered and concentrated under reduced pressure. The crude material was purified by column chromatography (10% 1M NH_3 in MeOH/DCM) to afford the title compound as a colourless oil (0.072 g, 35%). ^{1}H NMR (400 MHz, $CDCl_3$) δ 8.27 – 8.18 (m, 1H), 7.85 – 7.73 (m, 1H), 7.58 – 7.41 (m, 3H), 7.39-7.31 (m, Hz, 1H), 6.80 (d, *J* = 7.5 Hz, 1H), 6.56 (s, 1H), 5.30 (s, 1H), 4.45-4.25 (m, 1H), 4.25 – 4.08 (m, 2H), 3.48-3.41 (m, 2H), 3.41-3.33 (m, 2H), 3.12 -2.78 (m, 4H), 2.43-2.34 (m, 2H), 1.41 (s, 9H). ^{13}C NMR (101 MHz, $CDCl_3$) δ 172.52, 154.21, 134.63, 127.71, 126.65, 125.95, 125.58, 125.51, 121.85, 120.97, 105.11, 70.43, 51.78, 50.99, 48.95, 36.71, 28.54. LC-MS *m/z* calc. for $C_{23}H_{34}N_3O_5$ $[MH]^+$; 432.2, found; 432.2, t_R = 2.25 min.

(±)-3-((2-((2-Hydroxy-3-(naphthalen-1-yloxy)propyl)amino)ethyl)amino)-3-oxopropylamine ditrifluoroacetate (5)

To a solution of (±)-*tert*-butyl(3-((2-((2-hydroxy-3-(naphthalen-1-yloxy)propyl)amino)ethyl)amino)-3-oxopropyl)carbamate **(4)** (0.072 g, 0.17 mmol) in DCM (0.5 mL), TFA (0.5 mL) was added. The mixture was stirred at room temperature for 2 hours and the solvent was then removed under reduced pressure to afford the title compound as an off-white viscous solid which was used directly in the next step (0.054 g, 100%). LC-MS *m/z* calc. for $C_{23}H_{34}N_3O_5$ $[MH]^+$; 332.2, found; 322.1. LCMS t_R = 0.98 min.

(±)-*tert*-Butyl-(3-((3-((2-((2-hydroxy-3-(naphthalen-1-yloxy)propyl)amino)ethyl)amino)-3-oxopropyl)amino)-3-oxopropyl)carbamate (6)

The synthesis of the title compound **6** was carried out as described for (±)-*tert*-butyl(3-((2-((2-hydroxy-3-(naphthalen-1-yloxy)propyl)amino)ethyl)amino)-3-oxopropyl)carbamate **(4)**, using (±)-3-((2-((2-hydroxy-3-(naphthalen-1-yloxy)propyl)amino)ethyl)amino)-3-oxopropylamine ditrifluoroacetate **(5)**. The title compound was afforded as an off-white viscous solid (0.034 g, 41%). ^{1}H NMR (400 MHz, CD_3OD) δ 8.34 – 8.25 (m, 1H), 7.85 – 7.76 (m, 1H), 7.56 – 7.44 (m, 3H), 7.43 – 7.35 (m, 1H), 6.94 (dd, *J* = 7.6, 1.0 Hz, 1H), 4.53 - 4.43 (m, 1H), 4.26 (dd, *J* = 9.9, 5.0 Hz, 1H), 4.20 (dd, *J* = 9.9, 5.6 Hz, 1H), 3.58 – 3.41 (m, 4H),

3.36 – 3.34 (m, 2H), 3.29 – 3.24 (m, 4H), 2.44-2.26 (m, 4H). ^{13}C NMR (101 MHz, CD_3OD) δ 180.17, 155.35, 155.01, 136.08, 135.11, 130.26, 128.58, 127.51, 127.51, 126.92, 126.79, 126.28, 125.33, 122.79, 121.98, 118.74, 118.31, 106.16, 71.05, 66.84, 51.97, 45.82, 36.69. LC-MS *m/z* calc. for $C_{26}H_{39}N_4O_6$ $[MH]^+$; 503.3, found; 503.3, t_R = 2.25 min.

(±)-3-((3-((2-((2-Hydroxy-3-(naphthalen-1-yloxy)propyl)amino)ethyl)amino)-3-oxopropyl)amino)-3-oxopropylamine dihydrochloride (7)

Deprotection of (±)-*tert*-butyl-(3-((3-((2-((2-hydroxy-3-(naphthalen-1-yloxy)propyl)amino)ethyl)amino)-3-oxopropyl)amino)-3-oxopropyl)carbamate **(6)** (0.082 g, 0.16 mmol) was carried out as described for the synthesis of (±)-2-(2-Hydroxy-3-(naphthalen-1-yloxy)propyl-amino)ethylamine dihydrochloride **(3)**. The title compound was afforded as a white solid (0.019 g, 29%). ^{1}H NMR (400 MHz, CD_3OD) δ 8.35-8.26 (m, 1H), 7.92 – 7.74 (m, 1H), 7.57 – 7.43 (m, 3H), 7.39 (dd, *J* = 8.3, 7.5 Hz, 1H), 6.95 (d, *J* = 7.6 Hz, 1H), 4.48 (dtd, *J* = 9.8, 4.9, 3.0 Hz, 1H), 4.33 – 4.13 (m, 2H), 3.77 – 3.70 (m, 1H), 3.69 – 3.63 (m, 2H) 3.61 – 3.55 (m, 2H), 3.48 (t, *J* = 6.4 Hz, 3H), 3.41-3.32 (m, 1H), 3.18 (t, *J* = 6.5 Hz, 2H), 2.60 (t, *J* = 6.5 Hz, 2H), 2.45 (t, *J* = 6.5 Hz, 2H), 1.41 – 1.35 (m, 1H). ^{13}C NMR (101 MHz, CD_3OD) δ 175.66, 172.33, 155.40, 136.05, 128.54, 127.49, 126.93, 126.81, 126.28, 122.88, 121.90, 106.16, 71.15, 68.13, 66.86, 51.53, 37.16, 37.11, 37.06, 36.76, 33.00, 32.32. LC-MS *m/z* calc. for $C_{21}H_{31}N_4O_4$ $[M+H]^+$; 403.3, found; 403.3, t_R = 0.91 min.

***N*-(3-((3-((2-((2-Hydroxy-3-(naphthalen-1-yloxy)propyl)amino)ethyl)amino)-3-oxopropyl)amino)-3-oxopropyl)-6-((4-(2-(4,4-difluoro-4,4a-dihydro-5-(thiophen-2-yl)-4-bora-3a,4a-diaza-s-indacene-3-yl)vinyl)phenoxy)acetamido)-hexanamide (8, propranolol-β-Ala-β-Ala-X-BODIPY630/650)**

To (±)-3-((3-((2-((2-hydroxy-3-(naphthalen-1-yloxy)propyl)amino)ethyl)amino)-3-oxopropyl)amino)-3-oxopropylamine dihydrochloride **(7)** (2.2 mg, 4.54 µmol) in DMF (0.2 mL), DIPEA (1.98 µL, 11.40 µmol) was added and then BODIPY 630/650-X-SE (1.5 mg, 2.27 µmol) dissolved in DMF (0.8 mL) was added. The mixture was stirred with the exclusion of light for 3 hours. The solvent was removed under reduced pressure and the crude material was purified by semi-preparative HPLC (Method B) to give the title compound as a blue solid (2.0 mg, 91%). Analytical RP-HPLC t_R = 19.68 min, purity = 98% HRMS (ESI-TOF) *m/z* calc. for $C_{50}H_{57}BF_2N_7O_7S$ $[M+H]^+$; 948.4098 found; 948.4096 and 970.3929 [M+Na].

cDNA Construct.

The β2-adrenoceptor cDNA sequence (obtained from Missouri S&T cDNA Resource Centre; www.cdna.org) was PCR amplified to generate a β2-adrenoceptor sequence that was in frame with the BamH1 restriction site of sig-NLuc (Stoddart et al., 2015) and sig-SNAP

(Gherbi et al., 2015) and changed the start codon (Met) of the β2-adrenoceptor sequence to Leu. The primers used were: forward 5'-CCGCCGGATCCCTGGGGCAACCCGGGAACG-3' and reverse 5'-GGCGGGAATTCTTACAGCAGTGAGTCATTTG-3'. The PCR product was then ligated in frame into pcDNA3.1(+) containing sig.SNAP[3] or sig-NLuc[1] using BamHI and EcoRI restriction enzymes. This created the plasmids sig-SNAP-ADRB2-pcDNA3.1(+) and sig-NLuc-ADRB2-pcDNA3.1(+).

The pSIN-SNAP-ADRB2 construct was generated on the basis of pSIN-eGFP-BSD lentiviral vector (Dixon et al., 2011) as following: first, the pSIN-eGFP-BSD plasmid was digested with SpeI and EcoRI restriction enzymes in order to remove eGFP sequence and to produce the pSIN/BSD backbone; second, SNAP-ADRB2 fragment was PCR amplified with 5'-CTTAAACTAGTTACCGCCACCATGCGGCTCTGC-3' (forward) and 5'-TCTGCAGAATTCttacagcagtgagtcatttg-3' (reverse) primers using sig-SNAP-ADRB2-pcDNA3.1(+) as a template. The resulting PCR product was digested with SpeI and EcoRI restriction endonucleases and ligated into eGFP-free pSIN/BSD backbone. To make the pSIN-NLuc-ADRB2 construct, a NheI-EcoRI fragment containing the NanoLuc-ADRB2 fusion sequence was isolated from sig-NLuc-ADRB2-pcDNA3.1(+) and used to replace SpeI-EcoRI SNAP-ADRB2 sequence in pSIN-SNAP-ADRB2.

Cancer cell model.

This study used a highly metastatic variant of the female MDA-MB-231 triple-negative human breast cell line (MDA-MB-231^{HM}; a kind gift from Dr. Zhou Ou, Fudan University Shanghai Cancer Center, China) (Chang et al., 2008). Cell line identity was confirmed by short tandem repeat analysis. The cell line was stably transfected with the lentiviral vector pSIN-NLuc-ADRB2 encoding Nanoluc-β_2-adrenoreceptor (Nluc-β_2AR), using Fugene^{HD} reagent, following the manufacturer's protocol, using a 3:1 reagent:DNA ratio. Transfected cells were selected using 20 µg/mL blastocidin (Sigma). 10 µg/mL blastocidin was used for cell maintenance. Cells were cultured in Dulbecco's Modified Eagle Medium (DMEM) containing 2mM Glutamax (Gilbco) supplemented with 10% foetal bovine serum. For in vivo use, blastocidin was removed from the growth medium for several passages.

Confocal microscopy.

Confocal microscopy was performed using a Leica TCS SP8 inverted scanning microscope with a Zeiss 40x 1.3NA oil immersion HCPL APO CS2 objective lens. Untransfected MDA-MB-231^{HM} cells or MDA-MB-231^{HM} cells expressing NanoLuc-tagged β2-adrenoceptors were seeded in eight-well chambered coverslip slides (µSlide; Ibidi, Martinsried, Germany). Prior to imaging, media was replaced with Hank's buffered salt solution (HBSS) (Gibco, Thermo Fisher) pH 7.2-7.4, at 37°C. Cells were incubated in HBSS for 10 min with the nuclear stain

Hoechst 33342 (2 μg/mL), and then washed twice with HBSS. Cells were then treated with 50nM propranolol-(β-Ala-β-Ala)-X-BODIPY630/650, in the presence or absence of unlabelled propranolol (10μM), and incubated for 30 min at 37°C (without CO_2). Cells were washed with HBSS to remove unbound ligand before imaging. Nuclear labelling was detected using a 405nm-Argon laser line (415-470nm bandpass), and fluorescent ligand labelling was detected using a 633nm HeNe laser line and a 640-700 bandpass filter. Images were analysed using ImageJ 1.51 (Fiji, USA) software.

Widefield bioluminescence microscopy.

Bioluminescence imaging was performed using an Olympus LV200 Wide field inverted microscope, equipped with a 60x/1.42NA oil immersion objective lens. MDA-MB-231^{HM} cells transfected with NanoLuc-tagged human β_2-adrenoceptors were seeded into a 35mm MatTek dish containing a high tolerance 1.5μm coverslip. Before imaging, media was removed and cells were incubated with 2mL HBSS containing 400nM furimazine substrate (Promega) at 37°C, for 15 min. Background luminescence images were taken by capturing sequentially luminescence in the following channels: (1) open channel (20 sec exposure time); (2) DAPI channel (20 sec exposure time; 420nm longpass filter) and (3) Cy5 channel (4 min exposure time; 600/50nm bandpass filter). Cells were then incubated for 30 min with 50nM propranolol-(β-Ala-β-Ala)-X-BODIPY630/650, in the presence or absence of 10 μM ICI 118551, before images were acquired using the same acquisition sequence. BRET ratio measurements were performed using ImageJ 1.51 (National Institutes of Health, USA) and the time-series analyser V3 plugin.

***In vitro* NanoBRET assays.**

Saturation, competition and kinetics NanoBRET binding assays were performed on MDA-MB-231^{HM} cells stably expressing NanoLuc-tagged β2-adrenoceptors as described previously (Stoddart et al., 2015). Briefly, cells were seeded 24h before assay in white Perkin Elmer 96-well Isoplates. For experiments performed under equilibrium conditions, growth media was replaced with 100μL HBSS. Fluorescent and non-fluorescent ligands were added simultaneously and the 96-well plate was incubated for 1h at 37 °C (no CO_2). 10μL NanoLuc substrate furimazine (Promega) was then added to give a final concentration of 10μM and the plate was incubated for a further 5 minutes at 37 °C. For all experiments, the luminescence was measured using a CLARIOstar plate reader (BMG Labtech) with filtered light emission collected at 685nm/100nm bandpass (acceptor) and 460nm/80nm bandpass (donor) at room temperature. The raw BRET ratio was calculated by dividing the 685nm emission by the 460nm emission. The same experiments were also performed using the IVIS Lumina II whole-animal imaging system (Caliper Life Sciences, Perkin Elmer) using

both an open channel (donor; 1 sec exposure time) and the CY5.5 channel (acceptor; 660/20nm bandpass; 30 sec exposure time).

For kinetics binding assays, growth media from cells was replaced with 50μL HBSS containing 10μM furimazine substrate, and incubated for 15 min, at 37°C (without CO_2). 50μL ligands, previously prepared in HBSS, were then added to wells and luminescence measurements were made every minute (for 60 min) with the above emission settings on both the CLARIOstar plate reader and the IVIS Lumina II system as described above.

Breast cancer *in vivo* model.

$5x10^5$ (in 20μl PBS) MDA-MB-231^{HM} triple negative human breast cancer cells stably expressing Nanoluc-β_2-adrenoceptors were injected (Hamilton syringe with 26.5G needle) into the fourth left mammary fat pad of female BALB/c nu/nu immune-compromised mice (7-week-old) (University of Adelaide, Australia). Mice were housed under PC2 barrier conditions on a 12 h dark/light cycle and monitored daily. Primary tumours were measured by caliper and volume (mm^3) was calculated by the formula: (length x width^2)/2. Mice were maintained under 2-3% isoflurane anaesthesia during injections and imaging. All *in vivo* procedures were carried out at Monash Institute of Pharmaceutical Sciences according to protocols approved (MIPS.2012.11) by the Monash University Animal Ethics Committee and according to the NHMRC (Australia) guidelines.

Bioluminescence imaging to monitor tumour and metastasis development.

The growth of solid tumours and the extent of metastasis were monitored by whole-animal bioluminescence imaging. The luminescence from the NanoLuc-β2-adrenoceptors on MDA-MB-231^{HM} cells was monitored using an IVIS Lumina II camera system equipped with a heated stage (37°C). On the day of imaging, mice were anaesthetised with 2-3% isoflurane and then injected via the tail vein (i.v.) with 100μl Nano-Glo® luciferase substrate (furimazine, diluted in PBS; *circa* 0.37 mg/kg). Whole-animal images were taken 5 min after substrate injection (open channel; 30 sec exposure time). Immediately afterwards, images of metastasis localised in the thorax region were also taken. Images of the thorax were acquired 10 min after furimazine injection, using luminescence imaging (open channel; 2 min exposure time).

***In vivo* NanoBRET.**

i) Monitoring fluorescent ligand-receptor association in the primary tumour

In preliminary experiments to monitor ligand-receptor association *in vivo*, mice were firstly injected with 0.1 mg/kg Propranolol-(β-Ala-β-Ala)-X-630/650 (in 50μl of PBS) directly into the primary tumour (intratumoral; i.t). Immediately after fluorescent ligand injection, mice were

injected with 100μL 1:20 dilution furimazine substrate via the tail vein (i.v., 100μL diluted in PBS; *circa* 0.37 mg/kg) and imaged using the IVIS lumina II camera system. Mice were kept under 2-3% isoflurane anaesthesia during injections and imaging. Sequential luminescence (open channel, 30 sec exposure time) and fluorescence (Cy5.5. channel using 660/20nm bandpass filter; 5 min exposure time) images were taken every 6 min for a total time of 49 min. Images were acquired from 1 min after fluorescent ligand injection.

ii) Monitoring fluorescent ligand-receptor dissociation in the primary tumour

To monitor fluorescent ligand dissociation over-time in the primary tumour region, mice were administered with one of three different doses of Propranolol-(β-Ala-β-Ala)-X-630/650 (0.01, 0.03 or 0.1 mg/kg). At 1, 24, 48 and 72h after fluorescent ligand injection, mice were injected with furimazine substrate (i.v., 100μL in PBS, *circa* 0.37 mg/kg) and imaged 5 min later using the IVIS lumina II camera system. Sequential luminescence (open channel, 30 sec exposure time) and fluorescence (Cy5.5 channel, 5 min exposure times) images were acquired at 1h, 24h, 48h and 72h after fluorescent ligand injection (i.t.). All mice were also imaged on the day before fluorescent ligand injection, 5 min after 100μL i.v. injection with furimazine substrate (1:20 dilution in PBS) to determine luminescence (and BRET) baseline.

iii) Monitoring ligand-receptor engagement of unlabelled drugs administered locally in the primary tumour (i.t.) or via intravenous injection (i.v.)

To monitor specific ligand-receptor engagement of the unlabelled β_2-selective antagonist, ICI 118551, administered locally in the primary tumour (i.t.), mice were divided into two groups: Group 1 received an intra-tumour (i.t. 0.1 mg/kg; 50μL in PBS) injection of the fluorescent ligand alone and Group 2 received 0.3 mg/kg (i.t.; 50μL in PBS) ICI 118551 45 min prior to injection of 0.1 mg/kg Propranolol-BY630 (i.t.). 1h after the fluorescent ligand injection luminescence/fluorescence images were captured on the IVIS lumina II instrument (NanoLuc donor open channel, 30 sec exposure time; BRET acceptor Cy5.5 channel, 660nm/20nm band pass, 5 min exposure time), 5 min after furimazine injection (100μL in PBS; circa 0.37 mg/kg). Mice were imaged on the previous day 5 min after an equivalent furimazine i.v. injection to determine luminescence (and BRET) baseline. After 10 days, when fluorescent ligand was no longer detected by imaging, the treatment schedule was reversed. Group 1 mice were injected with 0.3 mg/kg ICI 118551 plus 0.1 mg/kg Propranolol-BY630/650, while Group 2 animals were injected with fluorescent ligand alone.

To investigate drug-receptor engagement in the primary tumour region following parenteral administration (i.v.) of the selective β_2-selective antagonist ICI 118551 (100μl in PBS; 10 mg/kg) a similar cross over experimental design was followed with 0.1 mg/kg propranolol-(β-Ala-β-Ala)-X-BODIPY630/650 injected directly into the primary tumour 45 min after i.v.

administration of ICI 118551. Mice were also imaged on the previous day, 5 min after i.v. injection of furimazine to determine luminescence (and BRET) baseline. Images were acquired as described above using the IVIS system, 5 min after furimazine substrate (100μL in PBS; 0.37 mg/kg) injection, using the same filter settings and exposure times as described above for the donor and acceptor readings.

Drug-receptor engagement in the primary tumour region was also investigated for a lower dose of ICI 118551 administered i.v. (1 mg/kg), as well as for an unlabelled β_1-selective antagonist, CGP20712A administered i.v. (10 mg/kg; 100μL in PBS). In these experiments, mice were administered with fluorescent ligand (0.1 mg/kg i.t.; 50μL in PBS). 45 min prior to fluorescent ligand injection, mice were administered (i.v.) with either PBS (100μL), CGP201712A (100μL; 10 mg/kg in PBS), or ICI 118551 (100μL; 1 mg/kg in PBS). Images were acquired 1h after fluorescent ligand injection, as described above. All mice were also imaged on the previous day, 5 min after i.v. injection with furimazine substrate (1:20 dilution, *circa* 0.37 mg/kg) to determine luminescence (and BRET) baseline. BRET ratios were calculated after dividing acceptor/donor emissions (photons/sec), determined using regions of interest (ROIs) drawn over the tumour site.

Data analysis.

***In vitro* pharmacological characterisation.**

For analysis of saturation binding data, raw BRET ratios obtained from each individual experiment were fitted using a non-linear regression equation shown below, using GraphPad Prism 7. Total and non-specific binding curves were fitted simultaneously using the following equation:

$$BRET\ Ratio = \frac{B_{max} \times [B]}{[B] + K_D} + \left((M \times [B]) + C\right)$$

where B_{max} is the maximal binding, [B] is the concentration of fluorescent ligand, K_D is the equilibrium dissociation constant, M is the slope of the non-specific binding component and C is the intercept with the Y-axis.

Competition binding curves were fitted to the following equation using Prism 7:

$$\%\ uninhibited\ binding = \frac{(100-NS)}{([A]/IC_{50})+1} + NS$$

where [A] is the concentration of unlabelled, IC_{50} is the molar concentration of the unlabelled ligand required to inhibit 50% of the specific binding of 50nM propranolol-(β-Ala-β-Ala)-X-BODIPY630/650 and NS represents non-specific binding.

The Cheng Prusoff equation was then used to convert IC_{50} values to absolute K_i values:

$$K_i = \frac{IC_{50}}{1+\frac{[L]}{K_D}}$$

where [L] is the concentration of labelled ligand and K_D is the dissociation constant of the fluorescent ligand obtained from saturation binding assays. pK_i values were then calculated as $-\log K_i$.

Data obtained for fluorescent ligand binding kinetics, using more than one concentration, were globally fitted to an association kinetics model. The kinetic rate constants: k_{off} (dissociation rate constant of the ligand; min^{-1}) and k_{on} (association rate constant; M^{-1} min^{-1}) were calculated from the following equation:

$$k_{on} = \frac{k_{obs} - k_{off}}{[L]}$$

where [L] is the fluorescent ligand concentration and k_{obs} is calculated from global fitting of the data to the following monoexponential association function:

$$Y = Y_{max}(1 - e^{-k_{obs}t})$$

where Y is the specific binding at time t, $Ymax$ corresponds to the level of specific binding at infinite time and k_{obs} is the rate constant for the observed rate of association.

***In vivo* data analysis.**

In vivo luminescence or fluorescence total flux (photons/sec) measurements were obtained using ROIs positioned on the primary tumour or thorax region, for primary tumour or metastasis measurements, respectively. Raw BRET ratios were calculated as:

$$BRET\ ratio = \frac{Acceptor\ Luminescence\ (CY5.5)}{Donor\ Luminescence\ (open\ channel)}$$

where acceptor luminescence (Cy5.5 channel) is measured as total flux (photons/sec) acquired using the Cy5.5 emission channel (660nm/20nm bandpass), and luminescence (open channel) is measured as total flux (photons/sec) acquired without using emission filters.

Statistical analysis.

For *in vitro* and *in vivo* studies, one-way or two-way ANOVA analysis with Tukey's or Dunnett's multiple comparison tests were used.

Supplemental References.

Chang, X.Z., Li, D.Q., Hou, Y.F., Wu, J., Lu, J.S., Di, D.H., Jin, W., Ou, Z.L., Shen, Z.Z., Shao, Z.M. (2008) Identification of the functional role of AF1Q in the progression of breast cancer. Breast Cancer Res. Treat. 111, 65–78.

Dixon, J. E. Dick, E., Rajamohan, D., Shakesheff, K.M., and Denning, C. (2011) Directed Differentiation of Human Embryonic Stem Cells to Interrogate the Cardiac Gene Regulatory Network. Molecular Therapy 19, 1695-1703.

Gherbi, K., May, L.T., Baker, J.G., Briddon, S.J., and Hill, S.J. (2015) Negative cooperativity across β_1-adrenoceptor homodimers provides insights into the nature of the secondary low affinity "CGP 12177" β_1-adrenoceptor binding conformation. *FASEB J*. 29, 2859-71.

Soave, M., Stoddart. L.A., Brown. A., Woolard. J., and Hill. S.J. (2016) Use of a novel proximity assay (BRET) to investigate the ligand binding characteristics of three fluorescent ligands to the human β1-adrenocpetor expressed in HEK-293 cells. Pharmacol. Res. Persp. 4: e00250.

Stoddart, L.A., Johnstone, E.K.M., Wheal, A.J., Goulding, J., Robers, M.B., Machleidt, T., Wood, K.V., Hill, S.J., and Pfleger KDG. (2015) Application of BRET to monitor ligand binding to GPCRs. Nature Methods, 12, 661–663.